Supporting Information

[Ag(L)NO_3] complexes with 2-benzoylpyridine-derived hydrazones: cytotoxic activity and interaction with biomolecules

Ane F. Santos,[a] Isabella P. Ferreira,[a] Carlos B. Pinheiro,[b] Verlane G. Santos,[c] Miriam T. P. Lopes,[c] Letícia R. Teixeira[a] , Willian R. Rocha [a], Gabriel L. S. Rodrigues[a] and Heloisa Beraldo*[a]

[a] Departamento de Química, Universidade Federal de Minas Gerais, Av. Presidente Antônio Carlos 6627, 31270-901, Belo Horizonte, MG, Brazil

[b] Departamento de Física, Universidade Federal de Minas Gerais, Av. Presidente Antônio Carlos 6627, 31270-901, Belo Horizonte, MG, Brazil

[c] Departamento de Farmacologia, Universidade Federal de Minas Gerais, Av. Presidente Antônio Carlos 6627, 31270-901, Belo Horizonte, MG, Brazil

*Corresponding author. Tel.: +55 (31)3409-5740.

E-mail address: hberaldo@ufmg.br

heloisaberaldoufmg@gmail.com (H. Beraldo)

Table of contents

The chemical structures of hydrazones and silver(I) complexes

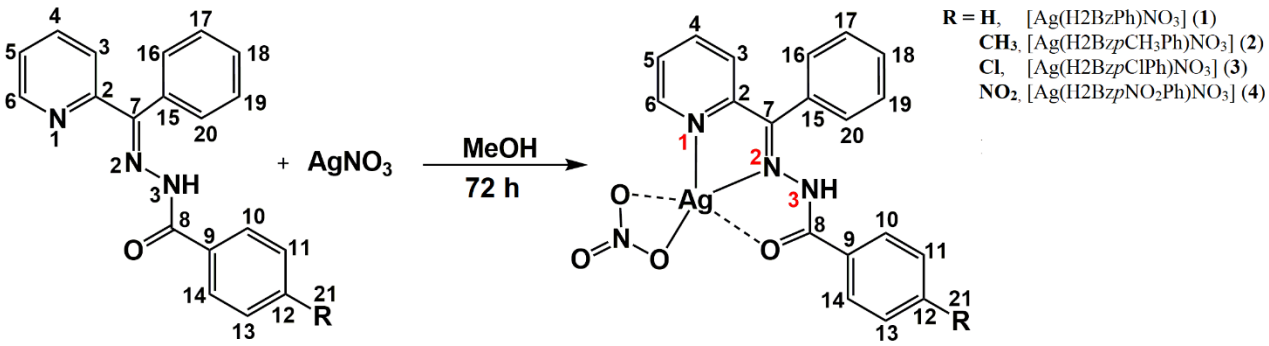

Figure S1. Syntheses of the silver(I) complexes with 2-benzoylpyridine-derived hydrazones and with the carbon atoms numbering scheme used in NMR.

Infrared spectra of 2-benzoylpyridine-benzoylhydrazones and their silver(I) [Ag(H2BzPh)NO_3] (**1**), [Ag(H2Bz*p*CH_3Ph)NO_3] (**2**), [Ag(H2Bz*p*ClPh)NO_3] (**3**) and [Ag(H2Bz*p*NO_2Ph)NO_3] (**4**) complexes

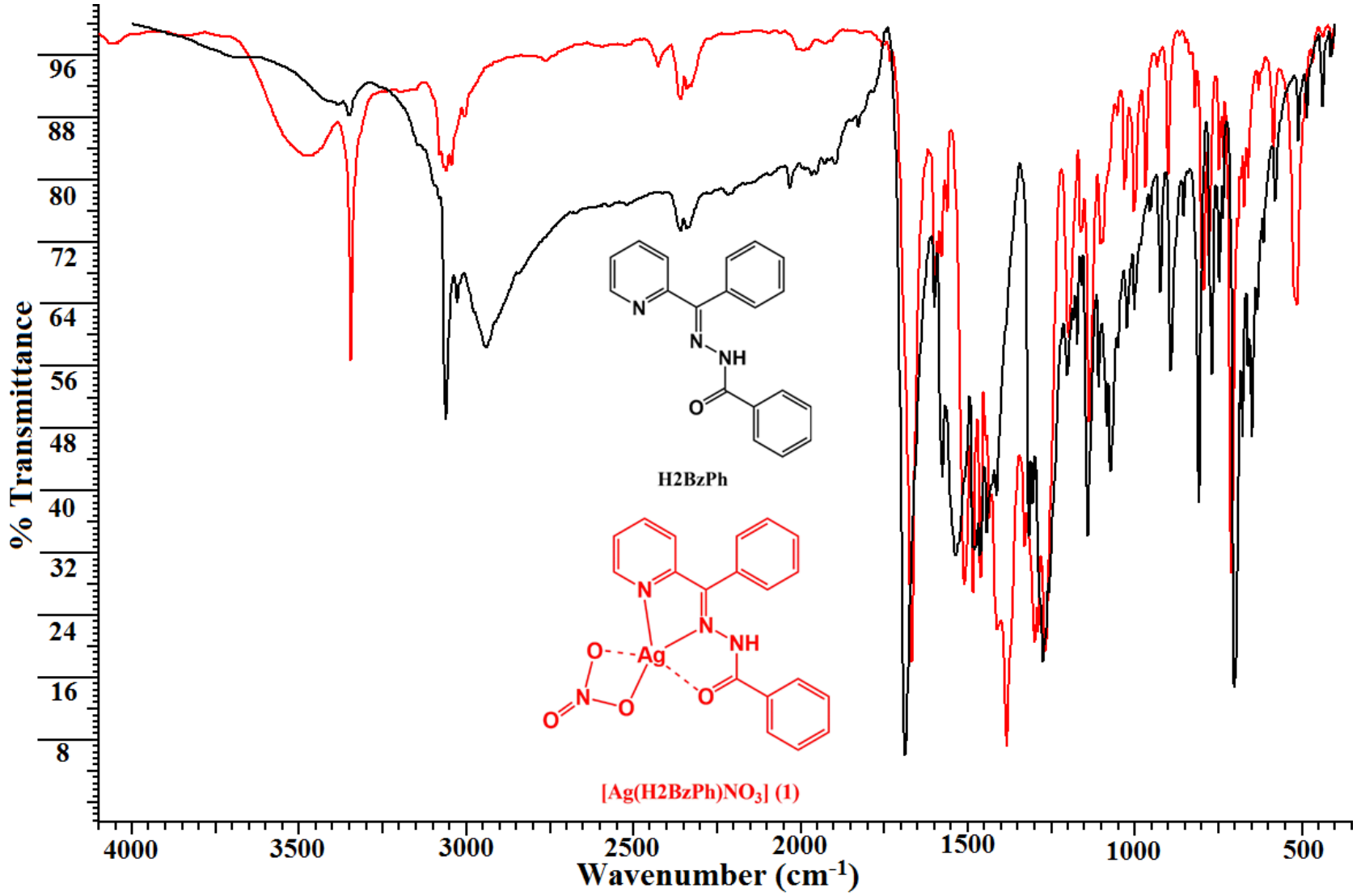

Figure S2. IR spectrum of H2BzPh (black line) and [Ag(H2BzPh)NO_3] (**1**) (red line) obtained in KBr pellets (4000-400 cm^{-1}).

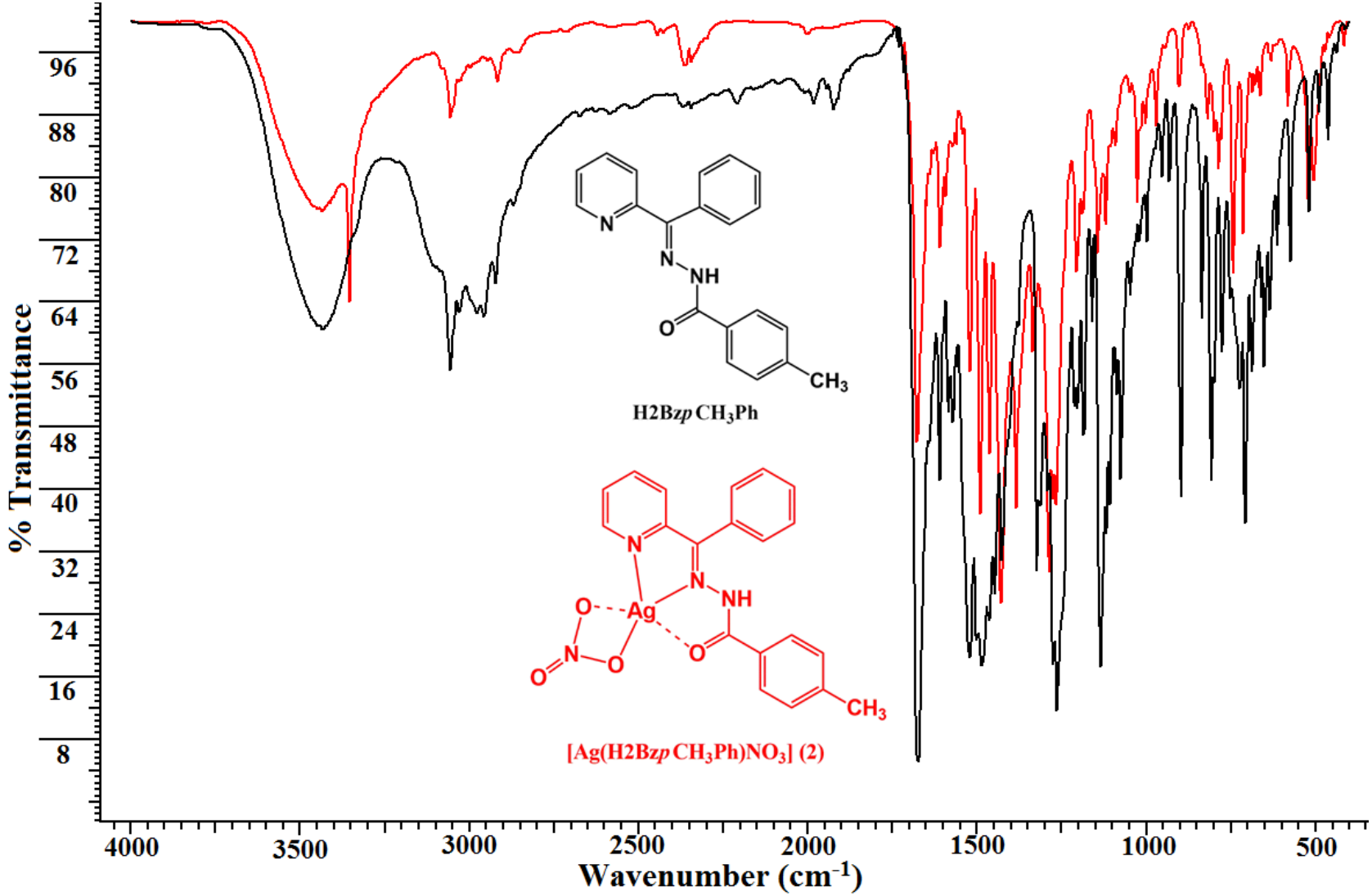

Figure S3. IR spectrum of H2Bz*p*CH_3Ph (black line) and [Ag(H2Bz*p*CH_3Ph)NO_3] (**2**) (red line) obtained in KBr pellets (4000-400 cm^{-1}).

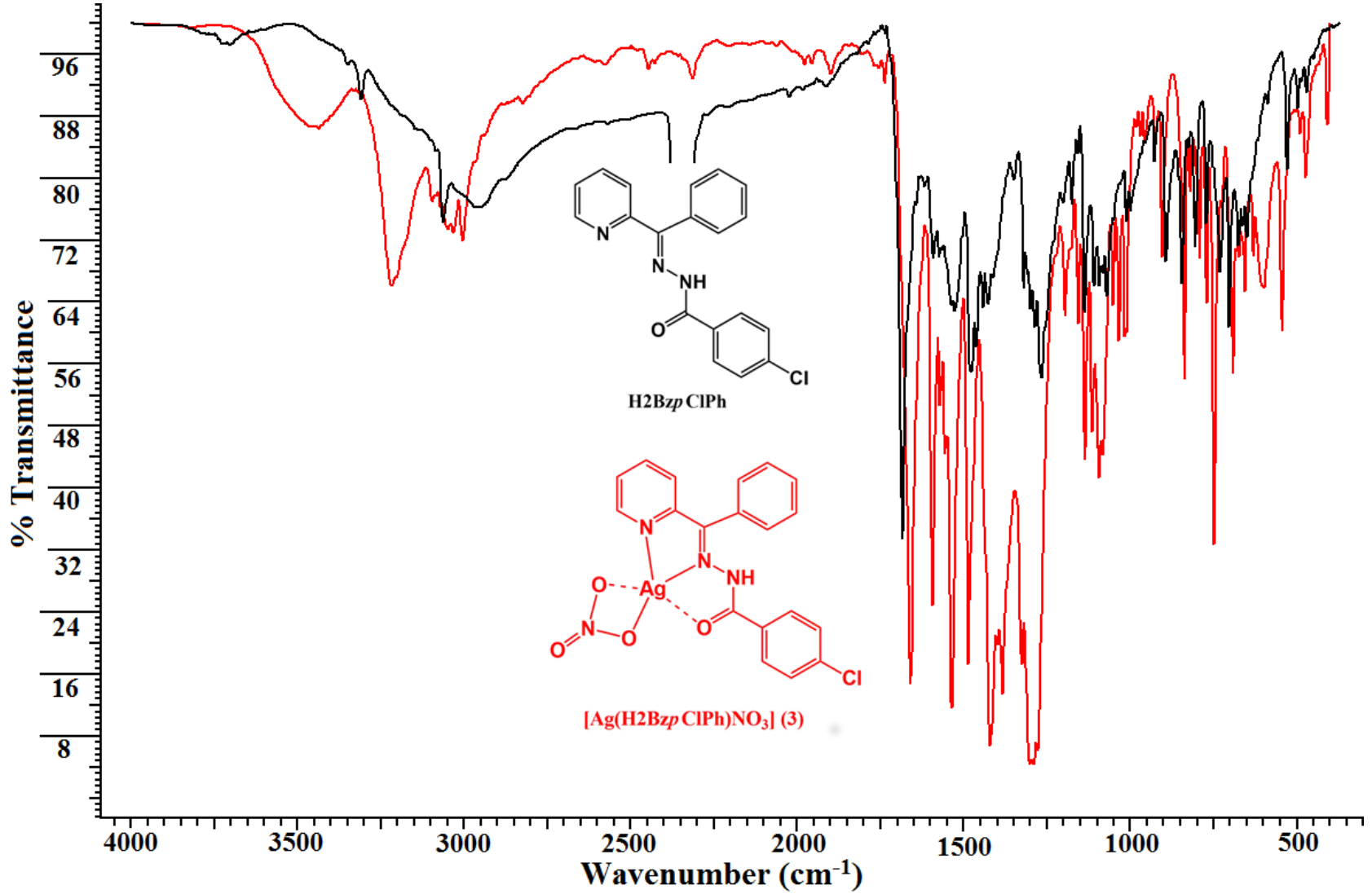

Figure S4. IR spectrum of H2Bz*p*ClPh (black line) and [Ag(H2Bz*p*ClPh)NO_3] (**3**) (red line) obtained in KBr pellets (4000-400 cm^{-1}).

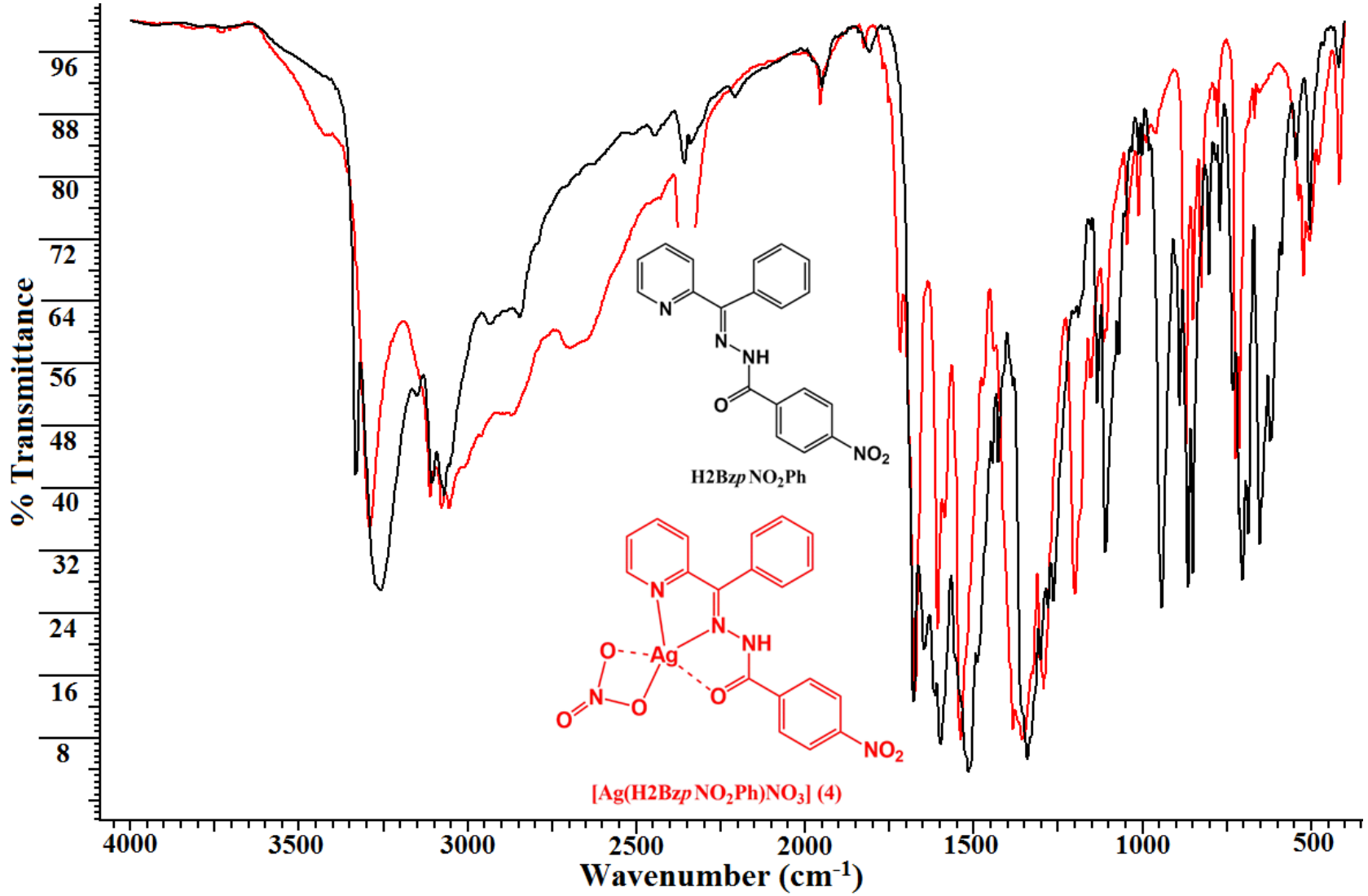

Figure S5. IR spectrum of H2Bz*p*NO_2Ph (black line) and [Ag(H2Bz*p*NO_2Ph)NO_3] (**4**) (red line) obtained in KBr pellets (4000-400 cm^{-1}).

^{1}H and ^{13}C NMR spectra of 2-benzoylpyridine-benzoylhydrazones and their silver(I) [Ag(H2BzPh)NO_3] (**1**), [Ag(H2Bz*p*CH_3Ph)NO_3] (**2**) and [Ag(H2Bz*p*ClPh)NO_3] (**3**) complexes

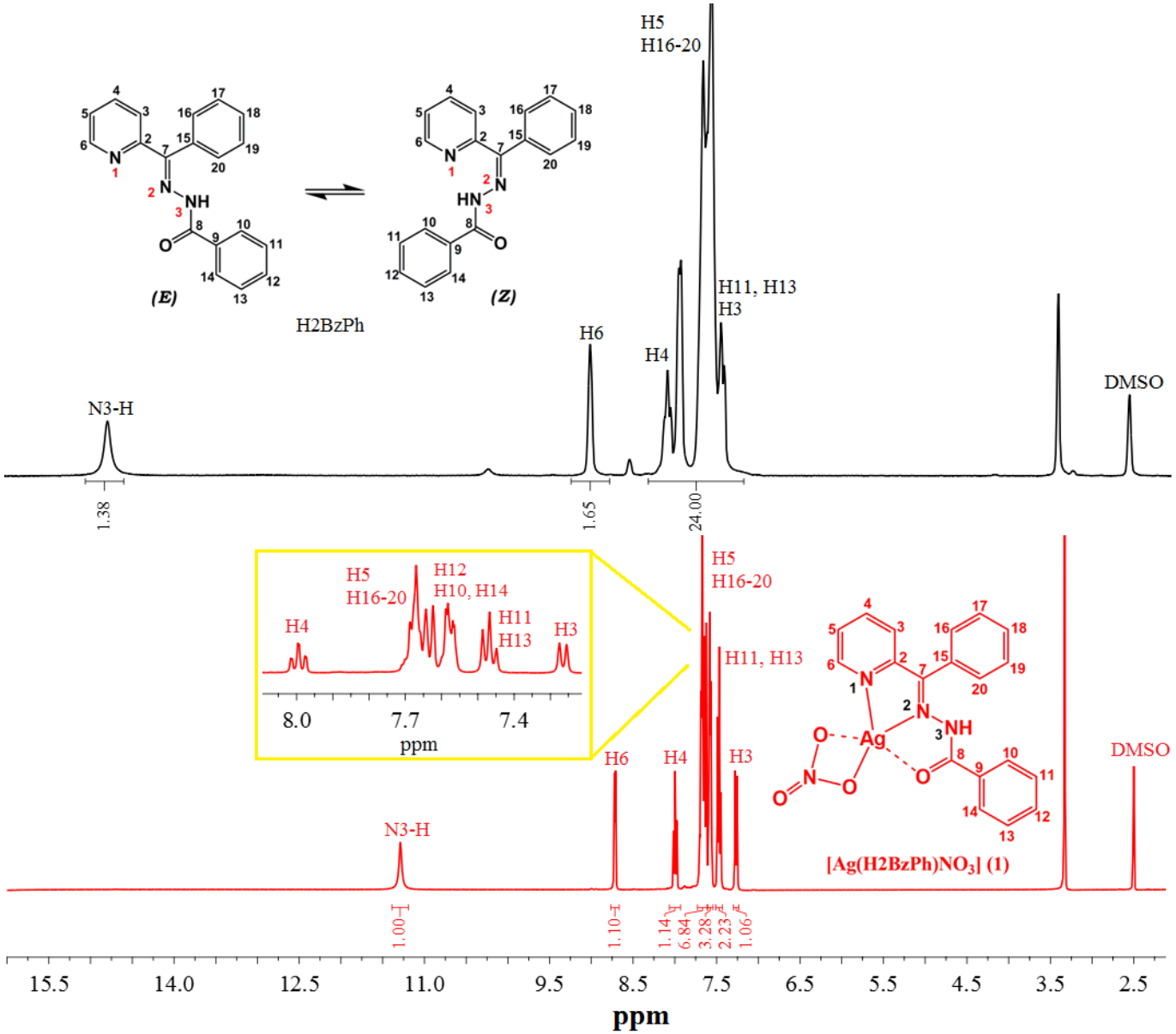

Figure S6. ^{1}H NMR spectrum of H2BzPh and [Ag(H2BzPh)NO_3] (**1**) in DMSO-d_6 (400 MHz) at room temperature.

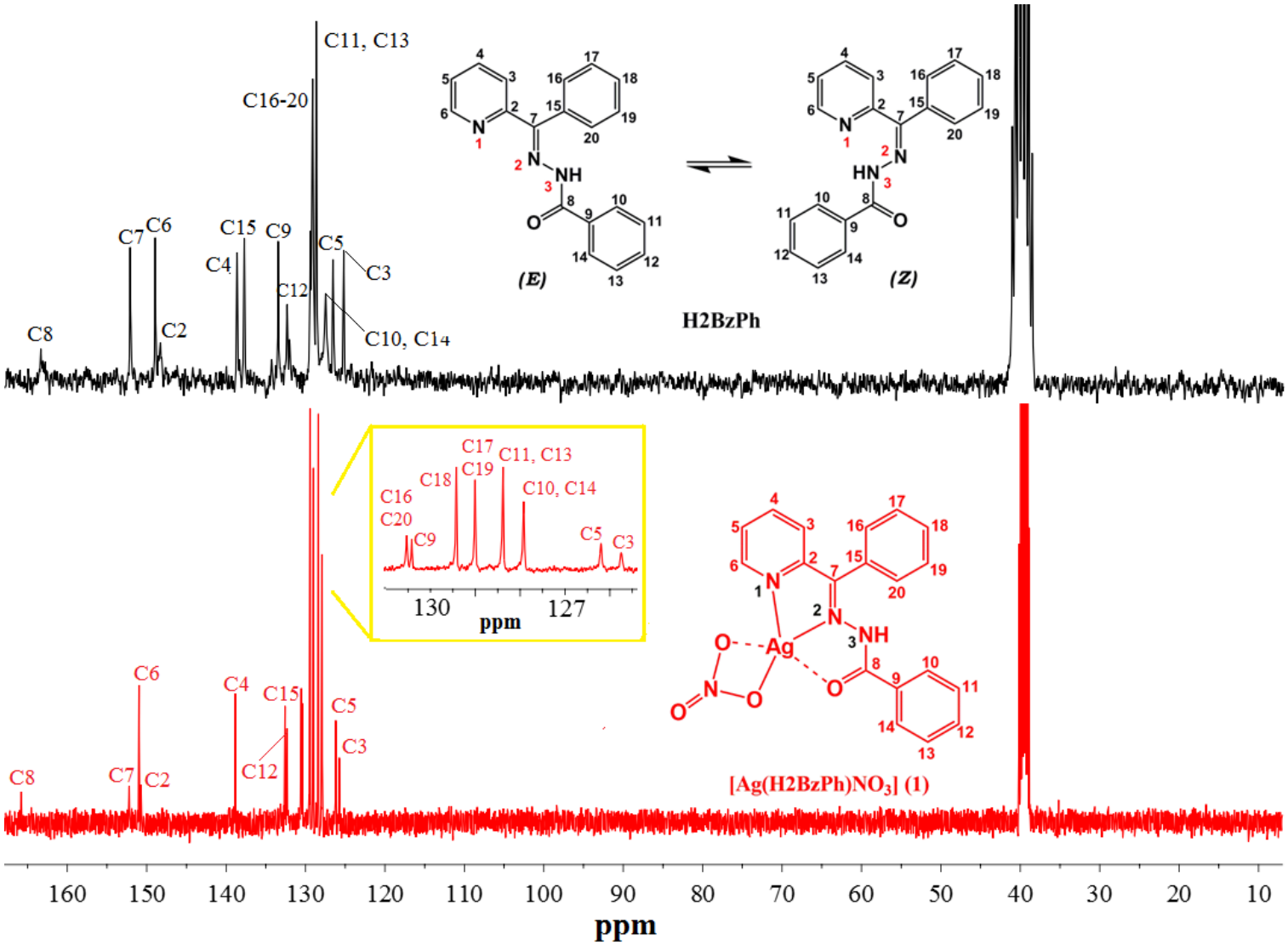

Figure S7. ^{13}C NMR spectrum of H2BzPh and [Ag(H2BzPh)NO_3] (**1**) in DMSO-d_6 (100 MHz) at room temperature.

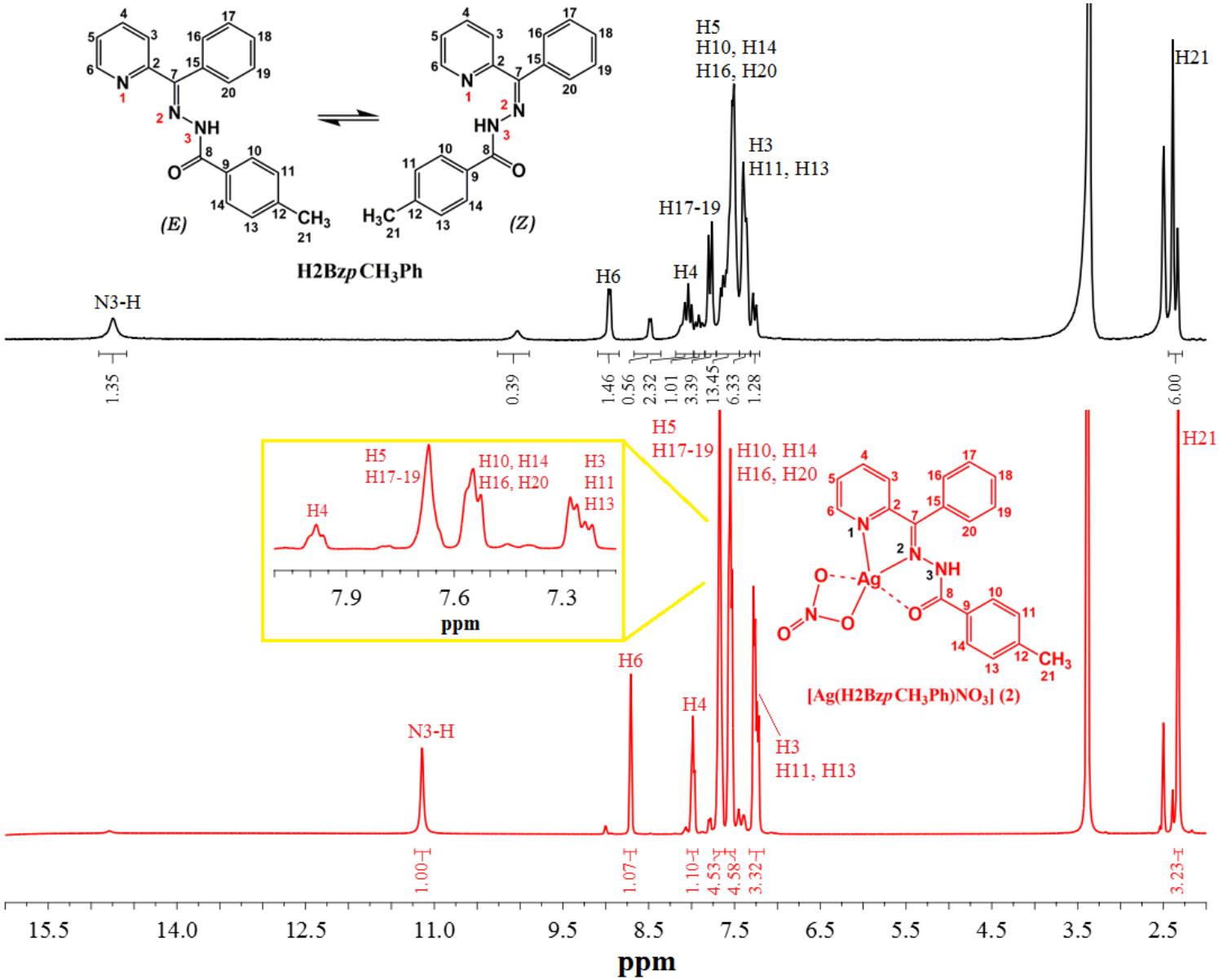

Figure S8. ^{1}H NMR spectrum of H2Bz*p*CH$_3$Ph and [Ag(H2Bz*p*CH$_3$Ph)NO$_3$] (**2**) in DMSO-d_6 (400 MHz) at room temperature.

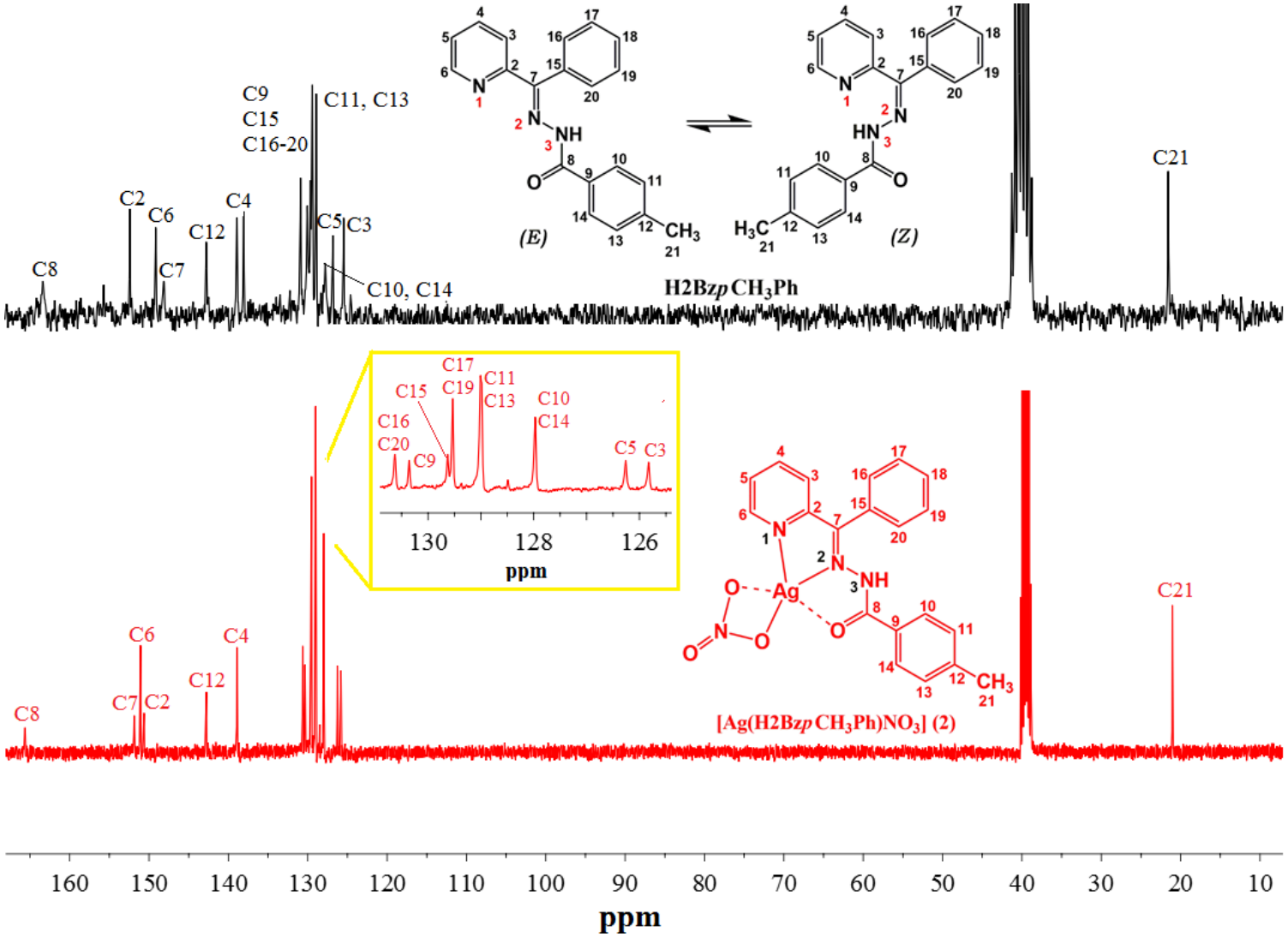

Figure S9. ^{13}C NMR spectrum of H2Bz*p*CH$_3$Ph and [Ag(H2Bz*p*CH$_3$Ph)NO$_3$] (**2**) in DMSO-d_6 (100 MHz) at room temperature.

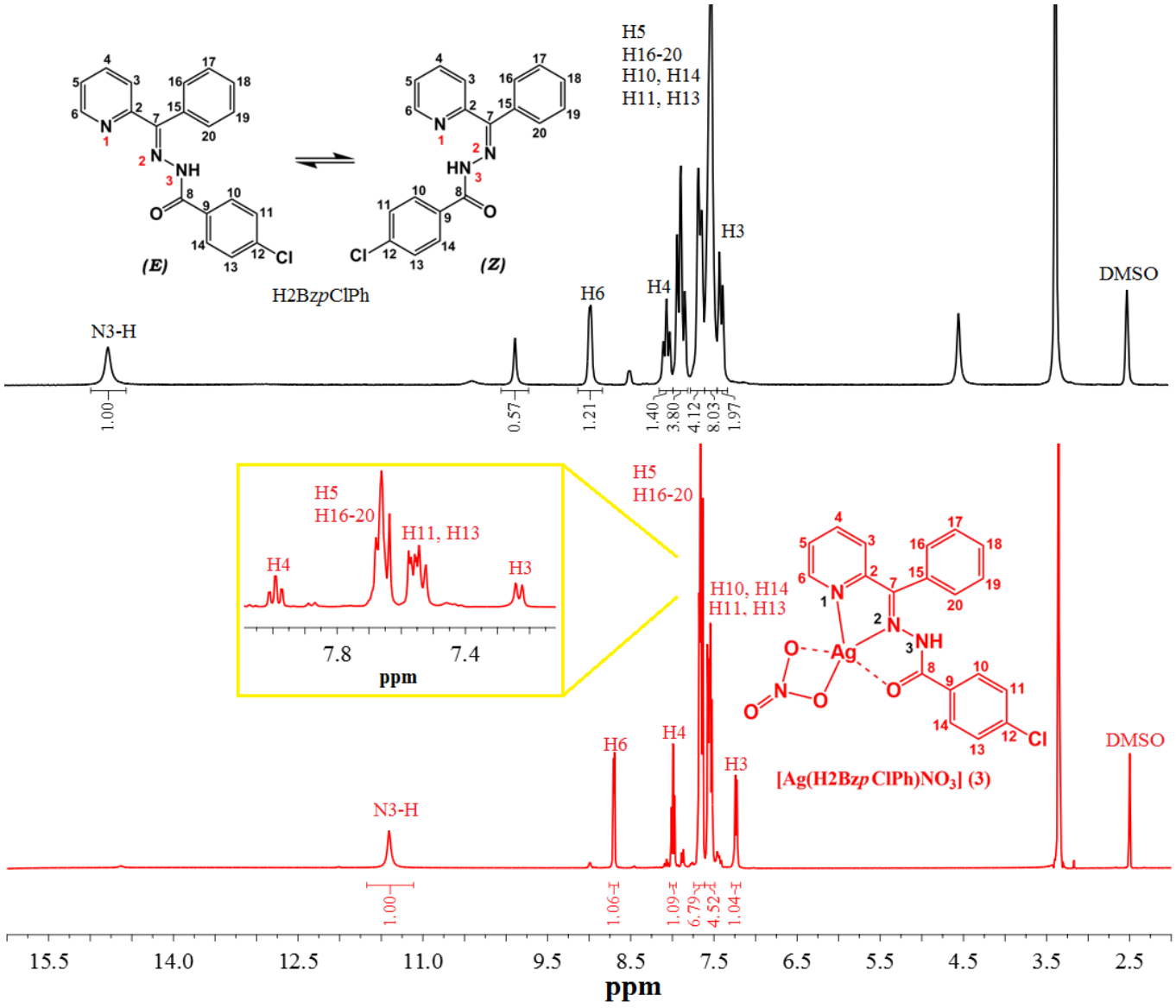

Figure S10. ^{1}H NMR spectrum of H2Bz*p*ClPh and [Ag(H2Bz*p*ClPh)NO_3] (**3**) in DMSO-d_6 (400 MHz) at room temperature.

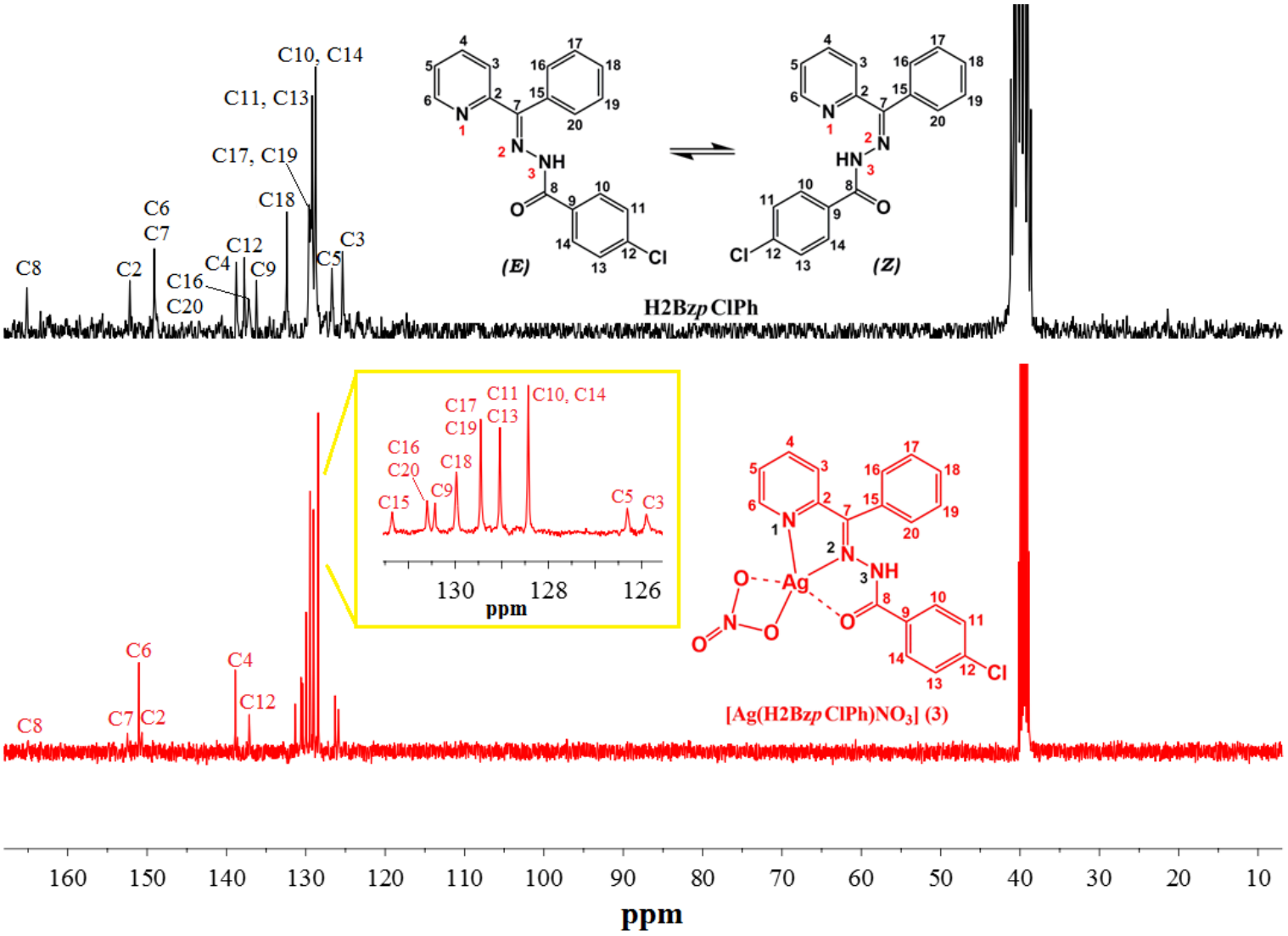

Figure S11. ^{13}C NMR spectrum of H2Bz*p*ClPh and [Ag(H2Bz*p*ClPh)NO_3] (**3**) in DMSO-d_6 (100 MHz) at room temperature.

X-ray crystallography

Table S1. Crystal data and structure refinement results for [Ag(H2BzPh)NO_3] (**1**), [Ag(H2Bz*p*CH_3Ph)NO_3] (**2**) and [Ag(H2Bz*p*ClPh)NO_3] (**3**).

Compound	(**1**)	(**2**)	(**3**)
Empirical formula	$C_{19}H_{15}N_4O_4Ag$	$C_{20}H_{17}N_4O_4Ag$	$C_{19}H_{14}ClN_4O_4Ag$
Molecular weight (g mol^{-1})	471.22	485.24	505.66
T (K)	100(2)	120(2)	270(2)
Crystal system	monoclinic	monoclinic	monoclinic
Space group	$P2_1/c$	I2/a	$P2_1/n$
Unit cell dimensions			
a (Å)	9.0545(2)	12.3045(5)	7.1699(4)
b (Å)	9.0588(2)	14.5456(7)	20.7822(10)
c (Å)	21.8960(5)	21.5645(8)	12.9758(7)
α (º)	90	90	90
β (º)	91.239(2)	97.044(4)	102.720(5)
γ (º)	90	90	90
V ($Å^3$)	1794.96(7)	3830.4(3)	1886.02(18)
Z	4	8	4
Density calculated (Mg m^{-3})	1.744	1.683	1.781
Absorption coefficient (mm^{-1})	1.158	1.088	1.246
F(000)	944	1952	1008
Crystal size (mm)	0.31 x 0.22 x 0.06	0.09 x 0.05 x 0.03	0.51 x 0.07 x 0.06
θ °range for data collection	2.25 to 29.55	1.69 to 26.37	1.88 to 26.37
Index ranges	$-11 \le h \le 12$	$-14 \le h \le 15$	$-8 \le h \le 8$
	$-12 \le k \le 12$	$-18 \le k \le 14$	$-25 \le k \le 25$
	$-29 \le l \le 29$	$-26 \le l \le 26$	$-16 \le l \le 16$
Reflections collected	46905	14044	29541
Independent reflections (R_{int})	4790 (0.051)	3925 (0.053)	3851 (0.066)
Completeness to θ = 25.242° (%)	100	100	100
Data/restraints/parameters	4790/0/253	3925/0/263	3851/0/262
Goodness-of-fit on F^2	1.096	1.023	1.046
Final R indices [I >2σ(I)]	R_1 = 0.0289,	R_1 = 0.0337,	R_1 = 0.0356,
	wR_2 = 0.0501	wR_2 = 0.0592	wR_2 = 0.0722
R indices (all data)	R_1 = 0.0458,	R_1 = 0.0515,	R_1 = 0.0644,
	wR_2 = 0.0571	wR_2 = 0.0648	wR_2 = 0.0862
Largest diff. peak and hole ($eÅ^{-3}$)	0.991 and -0.430	0.543 and -0.449	0.682 and -0.613

Computational Results

Structural results

The B3LYP/def2-sv(p) computed bond lengths involving the metallic center and the ligands are quoted in Table S2. Complex (**4**) dissociates in solution and therefore its bioactivities were not investigated. However, it was included in the theoretical studies. In general, there is a good agreement between the calculated and the experimental data, showing the reliability of the calculation method. In few cases there are more significant deviations between the computed and experimental values, being the highest 0.2 Å, which may be attributed to distortions due to packing effects in the solid phase.

Table S2. Calculated and experimental bond lengths around the metallic center for complexes (**1**-**4**) at the equilibrium geometry.

Ag-L bond lengths[a]	**Complex**							
	(**1**)		(**2**)		(**3**)		(**4**)	
	Calc.	Exp.[a]	Calc.	Exp.	Calc.	Exp.	Calc.	Exp.
O1	2.754	2.616(2)	2.729	2.711(2)	2.611	2.632(2)	2.653	N/A
N1	2.428	2.390(2)	2.451	2.365(2)	2.453	2.439(3)	2.494	N/A
N2	2.478	2.388(2)	2.467	2.388(2)	2.475	2.316(2)	2.417	N/A
O2	2.205	2.358(3)	2.228	2.279(2)	2.241	2.286(3)	2.285	N/A
O3	2.741	2.607(3)	2.661	2.774(2)	2.613	2.739(3)	2.462	N/A

[a]Experimental values obtained from X-ray diffraction measurements. All values in Angstrom

Among the Ag-O bond distances the Ag1-O2 bond is rather shorter for all complexes, indicating a stronger interaction between O2 of the nitrate ligand and the silver(I) center, since there is a high negative charge in the NO_3^- oxygens. However, O3 of nitrate remains much farther from the metallic center. The hydrazone O1 atom follows a similar pattern, and comparable Ag-O1 bond distances were found for all complexes. In complex (**4**) the Ag-O3 bond length is much shorter than

in the other complexes, probably due to the strong withdrawing effect of the nitro group, leading to much stronger NO_3^- coordination from both oxygens to the silver atom. Theoretical calculations described below indicated that the stronger the binding of nitrate to the silver center, the weaker the Ag-hydrazone coordination. These results may explain why in (**4**) decomplexation of the hydrazone ligand occurs in solution.

The hydrazone nitrogens form shorter bonds with silver, which is expected since they are softer than the oxygens, while Ag(I) is a soft cation.

Figure S12 illustrates the equilibrium geometry for (**1**).

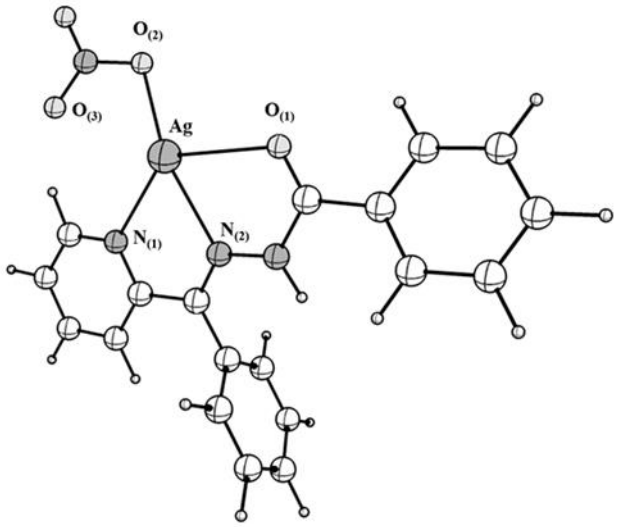

Figure S12. Equilibrium geometry of complex (**1**).

The potential energy surface (PES) generated for all complexes exhibits basically the same profile as that exemplified in Figure S13 for complex (**1**), indicating NO_3^- dissociation energy of ~ 30 kcal mol^{-1} in gas phase. Figure S13 also shows one interesting characteristic observed for all complexes. As the NO_3^- ligand dissociates from the metallic center, the distances between the oxygen of the hydrazone and the metal diminishes. Indeed, as the NO_3^- ligand dissociates, coordination of the hydrazone to the metallic fragment becomes stronger, with decrease in all M-L bond distances.

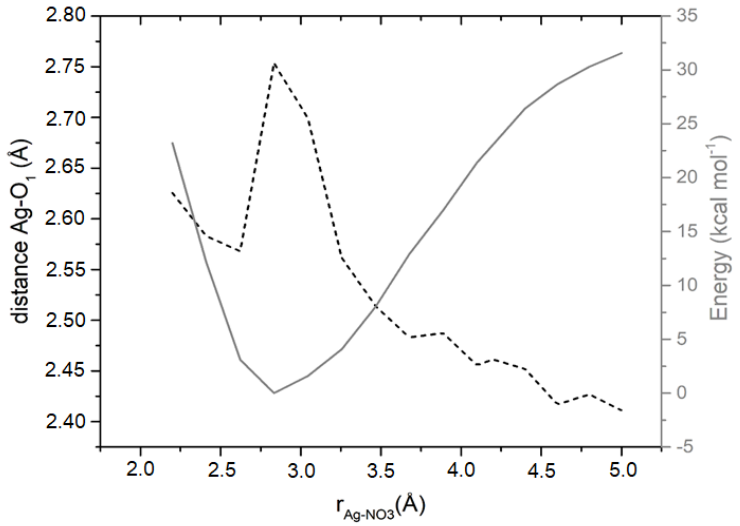

Figure S13. Potential Energy Surface for the dissociation of NO_3^- from complex (**1**). The horizontal axis indicates the distance between the silver atom and the nitrogen atom of the nitrate. The right vertical axis shows the variation of electronic energy relative to the equilibrium structure (full line) and the left vertical axis shows the bond length between silver and the oxygen from the hydrazone (dashed line), O1.

Table S3 shows structural parameters for complex (**1**) in different points of the PES. The results reveal that although the dissociation process of NO_3^- is not favorable, the Ag(I) ion tends to adopt a tri-coordinated arrangement in the complexes to acquire thermodynamic stability.

Table S3. Bond lengths between the silver and all the coordinated atoms of the ligands obtained for each point of the PES for complex (**1**).[a]

Ag-L bond lengths[b]	r(Ag-NO_3^-)					
	2.830	2.530	3.200	3.870	4.530	5.200
O1	2.729	2.584	2.610	2.489	2.471	2.440
N1	2.451	2.633	2.487	2.437	2.367	2.308
N2	2.467	2.422	2.432	2.429	2.409	2.415

O2	2.228	2.231	2.260	2.631	3.279	4.007
O3	2.661	2.320	3.296	4.347	5.034	5.522

[a]The PES was constructed by varying the r(Ag-NO_3^-) distance as mentioned in the computational details section. [b]Ag-L refers to the bond lengths involving the ligand atoms and the silver(I). All values are in Angstrom.

Table S4 shows the Mayer Bond Order involving the atoms coordinated to the metallic center in the complexes, in their equilibrium, with NO_3^- free geometries. The Ag-L bond orders range from 0.1 to 0.3, which are small values compared with those found for covalent bonds, indicating bonds with probably high electrostatic character. These values are, however, somewhat common for coordination compounds in which the central metal has d^{10} electronic configuration. For comparison, calculations at the same MP2 level of theory for simple complexes of Zn(II) and Cu(I) with water or ammonia provided Zn(II)-N bond order of 0.35 in $[Zn(NH_3)_4]^{2+}$ and of 0.30 for Zn(II)-O bond order in $[Zn(H_2O)_4]^{2+}$. Calculations for Cu(I) complexes $[Cu(NH_3)_3]^+$ and $[Cu(H_2O)_2]^+$ resulted in values of 0.30 and 0.23 for the Cu(I)-N and Cu(I)-O bonds, respectively. Therefore, the calculated Mayer bond order values for the Ag(I)-hydrazone complexes under study are just slightly smaller than those found for the Zn(II) and Cu(I) d^{10} complexes. However, it is worth noticing that the Ag(I) complexes have a chelate ligand and, therefore, the atoms coordinated to the metallic center do not have the same spatial freedom as the monodentate ligands. Therefore, they give rise to more distorted metal-ligand bonds, with smaller bond orders.

It is worth noticing that all bond orders involving the metal and the atoms from the hydrazone ligand increase significantly when NO_3^- dissociates, showing again that the bonding of nitrate leads to the weakening of all other interactions in the coordination sphere of the metal. Interestingly, in most of the complexes the bond order between the oxygen from the hydrazone and the silver center in the minimum energy geometry is zero (non-existent).

Table S4. Mayer Bond Order between the coordinated atoms of the ligands and the silver center for all complexes in their minimum (min.) and nitrate dissociated (diss.) geometries of the PES.

Complex	Geometry	Atom Bonded to the Metallic Center				
		O1	N1	N2	O2	O3
(**1**)	min.	0	0.16	0.12	0.34	0.12
	diss.	0.16	0.27	0.12	-	-
(**2**)	min.	0	0.16	0.12	0.33	0.13
	diss.	0.16	0.28	0.12	-	-
(**3**)	min.	0.10	0.14	0.12	0.31	0.14
	diss.	0.16	0.27	0.13	-	-
(**4**)	min.	0	0.13	0.13	0.28	0.18
	diss.	0.14	0.27	0.14	-	-

Nature of the bonds

Table S5 shows the calculated values of $\rho(r)$, $V(r)$, $H(r)$, $\nabla^2\rho(r)$, $\varepsilon(r)$, and $\eta(r)$ for the optimized geometries of the complexes, computed at the bond critical points (BCP) between silver and the coordinated atoms of the ligands. Except for complex (**2**), all other complexes show positive values of the Laplacian in all BCPs, together with values of $\eta(r)$ smaller than 1, characterizing closed-shell interactions. These results are expected for d^{10} cations like Ag(I), since they have all d orbitals occupied, and thus are incapable of acting as electron receptors in electronic covalent sharing, thus resulting in interactions with strong electrostatic character.

For all complexes in all selected geometries there is a BCP between the axis linking the Ag atom and the O atom from the hydrazone. This indicates the presence of a bonded interaction between these two atoms even for the large distances found at the minimum geometries, in which the two atoms are separated by distances around 2.65 Å. In the equilibrium geometries, calculations also show BCPs between both oxygens of the nitrate and the silver atom, indicating that NO_3^- coordinates to the Ag center in a bidentate fashion, although the second coordination is not very stable.

The electron density at the BCP is a measure of the bond strength. In this regard, Table S5 also shows the higher bond strength between Ag(I) and the oxygen atoms of nitrate, compared to the other coordinated atoms, since in this BCP $\rho(r)$ has the largest values. In addition, the value of $\varepsilon(r)$ at the BCP of one of the NO_3^- oxygens tends to be much larger than the value for the second oxygen. This reflects a distorted and unstable bond, which is expected because the angle between the nitrate oxygens and the silver atom is very inappropriate for chelating coordination.

Complex (**2**) presented a set of different characteristics. For (**2**) the Laplacian in all the BCPs is negative, which is an indication of the high contribution of the potential over the kinetic energy density, consequential of a larger covalent bond character. The $\eta(r)$ values also support this statement as they are all significantly larger than unit in all BCPs. These effects might be due to the electron-donation character of the *para*-methyl group of the hydrazone ligand in complex (**2**).

Table S6 shows the QTAIM analysis performed along the PES only for complex (**2**). The values of $\nabla^2\rho(r)$ and $\eta(r)$ at the BCPs are positive and larger than one, respectively, and together with $H(r)$ values very close to zero, they reinforce the electrostatic nature of the Ag-L bonds. Dissociation of the NO_3^- ligand leads to an increase in electron density at the BCPs of the three remaining coordinated atoms. For example, $\rho(r)$=0.19, when NO_3^- is at 2.530 Å from Ag (P2), and $\rho(r)$=0.26 when NO_3^- is farthest (5.200 Å, P10) in the Ag-O1 BCP. These results show that as NO_3^- dissociates, the interaction between the hydrazone and the metallic center becomes stronger.

Table S5. Calculated electron density properties at the bond critical point (BCP) involving Ag and the indicated atoms of the ligands, in the equilibrium geometry of complexes (**1-4**).[a]

Complex	Property	Atom Bonded to the Metallic Center				
		O1	N1	N2	O2	O3
(**1**)	$\rho(r)$	0.13	0.28	0.32	0.47	0.15
	$V(r)$	-0.02	-0.05	-0.06	-0.11	-0.02
	$H(r)$	0.00	0.00	-0.01	-0.01	0.00
	$\nabla^2\rho(r)$	2.00	3.89	4.40	7.74	2.23
	$\varepsilon(r)$	0.06	0.05	0.04	0.05	3.44
	$\eta(r)$	0.15	0.17	0.18	0.18	0.16
(**2**)	$\rho(r)$	1.84	1.94	2.14	1.94	2.17
	$V(r)$	-0.34	-0.37	-0.49	-0.37	-0.50
	$H(r)$	-0.27	-0.33	-0.37	-0.33	-0.38
	$\nabla^2\rho(r)$	-18.58	-27.40	-25.19	-27.35	-25.70
	$\varepsilon(r)$	0.14	0.01	0.19	0.01	0.19
	$\eta(r)$	1.77	1.74	2.86	1.75	2.94
(**3**)	$\rho(r)$	0.18	0.28	0.30	0.43	0.19
	$V(r)$	-0.03	-0.05	-0.05	-0.09	-0.03
	$H(r)$	0.00	0.00	-0.01	-0.01	0.00
	$\nabla^2\rho(r)$	2.88	3.95	4.15	7.13	2.92
	$\varepsilon(r)$	0.02	0.07	0.05	0.05	0.21
	$\eta(r)$	0.15	0.17	0.18	0.18	0.15
(**4**)	$\rho(r)$	0.16	0.32	0.27	0.39	0.26
	$V(r)$	-0.02	-0.06	-0.05	-0.08	-0.05
	$H(r)$	0.00	-0.01	0.00	-0.01	0.00
	$\nabla^2\rho(r)$	2.58	4.51	3.81	6.41	4.19
	$\varepsilon(r)$	0.03	0.07	0.05	0.05	0.02
	$\eta(r)$	0.15	0.18	0.17	0.17	0.16

[a]All values in a.u. The meaning of each computed property is described in the theoretical details section

Table S6. Calculated electron density properties at the bond critical point (BCP) between Ag and the indicated atom of the ligands. The values were obtained for complex (**2**) in two geometries of the PES, the point P2 and the last point P10 when the NO_3^- is farthest from the metal.

Property[a]	Atom Bonded to the Metallic Center									
	O1		N2		N1		O2		O3	
	P2	P10	P2	P10	P2	P10	P2	P10	P2	P10
$\rho(r)$	0.19	0.26	0.31	0.32	0.21	0.42	0.44	-	0.35	-
$V(r)$	-0.03	-0.05	-0.06	-0.06	-0.03	-0.08	-0.10	-	-0.07	-
$H(r)$	0.00	0.00	-0.01	-0.01	0.00	-0.01	-0.01	-	-0.01	-
$\nabla^2\rho(r)$	3.08	4.32	4.48	4.51	2.78	5.47	7.39	-	6.07	-
$\varepsilon(r)$	0.01	0.00	0.09	0.06	0.03	0.04	0.03	-	0.07	-
$\eta(r)$	0.15	0.16	0.18	0.18	0.17	0.19	0.17	-	0.16	-

[a] The meaning of each computed property is described in the theoretical detail section. All values in a.u.

Figure S14 shows a 2-D plot of $\nabla^2\rho(r)$ at the equilibrium geometry of complex (**2**). Despite the negative values of $\nabla^2\rho(r)$ shown in Table S5, at the BCPs involving the coordinated atoms the region between silver and its surrounding atoms is a region of positive $\nabla^2\rho(r)$ (full lines in Figure S14), and consequently a region of electron density depletion, characteristic of closed-shell interactions.

The 2-D and 3-D color scaled maps shown in Figures S15 and S16 provide further support for this conclusion. Figure S15 shows regions of low electron density for complex (**2**) in the surroundings of the Ag atom, or regions which are close to the atoms coordinated to the metal, where $\rho(r)$ is displaced upon nitrate dissociation. One can observe that the surroundings of the Ag atom have higher electron density when the NO_3^- ligand is dissociated. From the electron density map represented in

Figure S16, it is possible to observe that $\rho(r)$ is displaced to regions near the atoms connected to silver when NO_3^- is not coordinated.

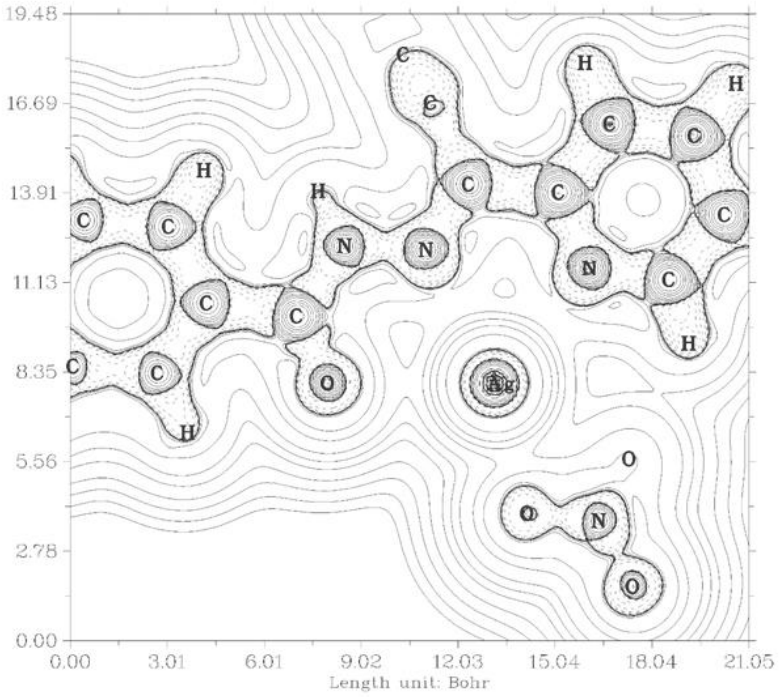

Figure S14. 2-D plot of $\nabla^2\rho(r)$ for the minimum energy geometry of complex (**2**). The dashed lines indicate a negative value of $\nabla^2\rho(r)$ and hence a region of charge accumulation, while the full lines indicate a positive value of $\nabla^2\rho(r)$ and therefore a region of charge depletion.

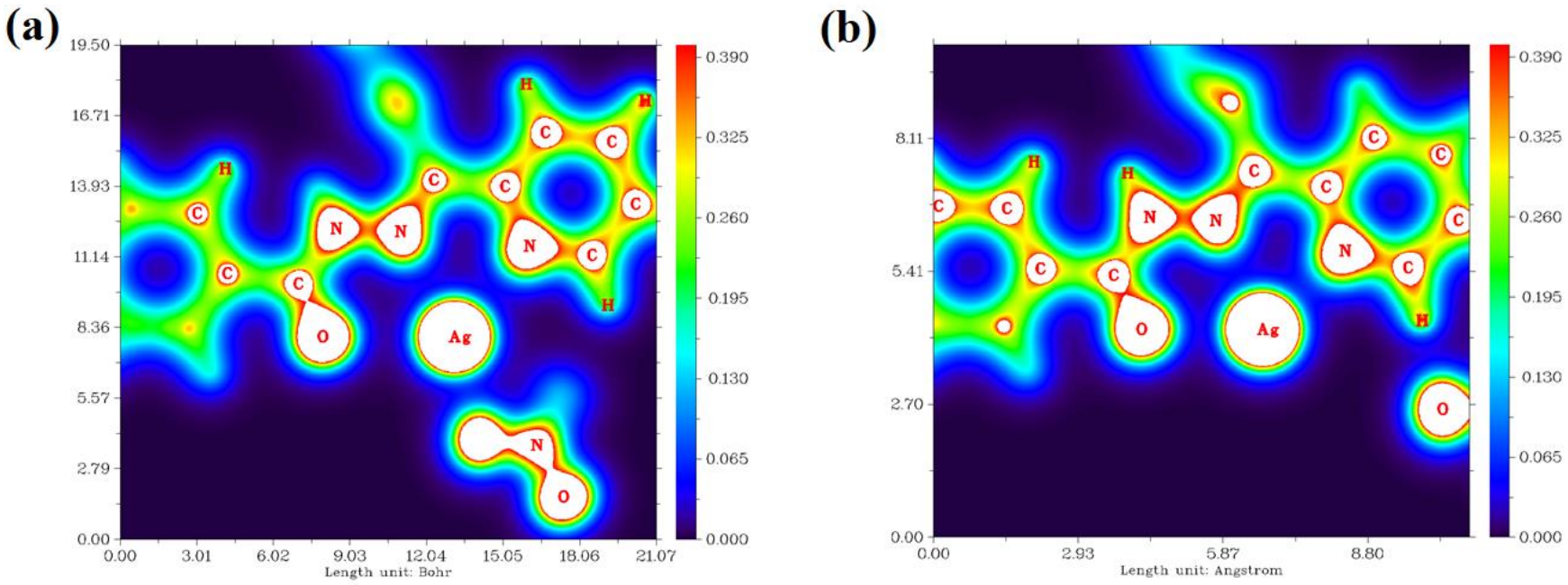

Figure S15. 2-D plot of the electron density for the minimum energy structure (a) and the structure in which the NO_3^- is dissociated from the Ag center (b) of the complex (**2**). The red and blue areas denote regions of high and low electron density, respectively, while the blank areas indicate large electron densities out of scale.

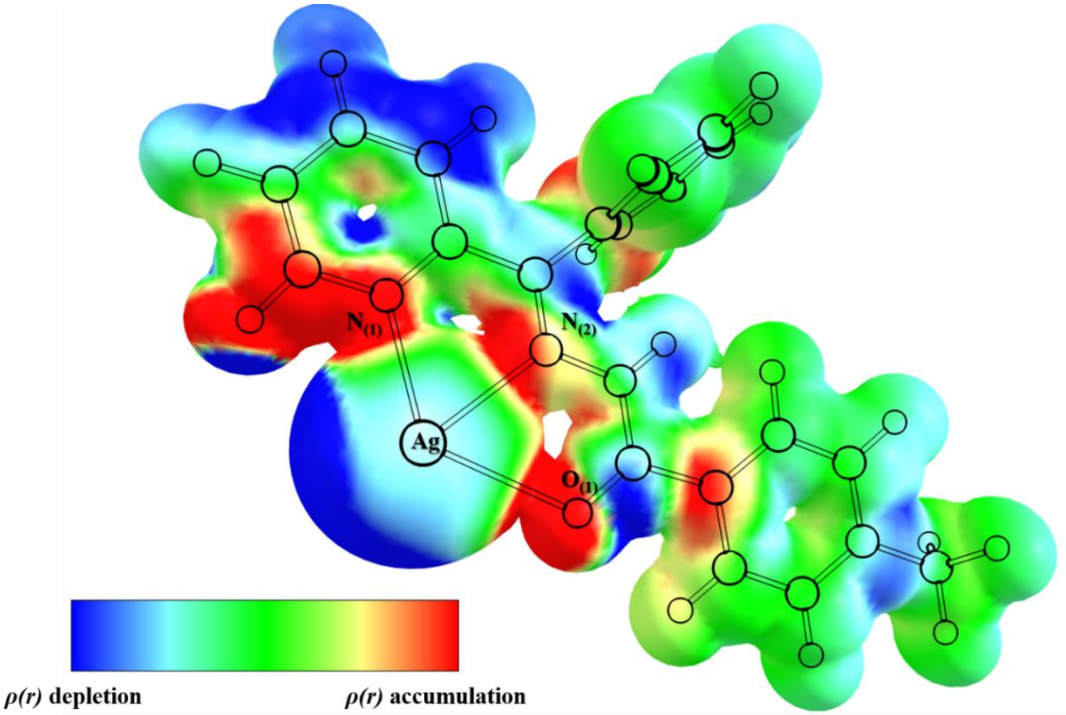

Figure S16. 3-D plot of the difference in electron density for the equilibrium geometry of the complex (**2**). with and without the NO_3^- ligand. The red surfaces indicate where the electron density is displaced to when the nitrate dissociates (higher *ρ(r)* in dissociated form) whilst the blue surfaces indicate where the electron density is removed upon nitrate dissociation (lower *ρ(r)* in dissociated form). In the green region the electron density remains unchanged.

Theoretical calculations

Computational Details

Full geometry optimizations of the complexes were performed at the Density Functional Theory level (DFT)[1] employing the hybrid B3LYP exchange-correlation functional.[2] The atoms of the ligands were treated with the def2-SV(P) split valence, double-zeta plus polarization basis set, from Ahlrichs and Wigend.[3] For the Ag atom, the 28 core electrons were replaced by the def2-ECP pseudopotential[4] and the valence electrons were also treated with the Def2-SV(P) basis set. To speed up calculations, the Resolution of Identity (RI)[5] algorithm was used for the Coulomb term of the Fock Matrix in conjunction with the Chain of Spheres (COSX)[6] approach for the exchange part, employing the def2/J[7] general auxiliary basis set.

In order to investigate energetics of the interaction between the NO_3^- ligand and the metallic fragment, Potential Energy Surfaces (PES) were constructed for each of the complexes under study, employing the same level of theory used in the geometry optimizations. The NO_3^- species was kept with constrained internal geometry and the distance between its center of mass with respected to the Ag atom was varied from 2.2 to 5.2 Å in 10 steps, with full geometry optimization at each step.

To better understand the nature of the interactions involving the metallic center and the ligands, the topology of the electronic density was analyzed using the Quantum Theory of Atoms in Molecules (QTAIM)[8] as implemented in the Multiwfn[9] software. These QTAIM analyses were carried out from single point Spin-component Scaled Second Order Perturbative (SCS-MP2)[10,11] calculations, including relativistic corrections, using the standard second-order Douglas-Kroll-Hess[12,13] procedure. For the light atoms, the MP2 calculations used the correlated-consistent cc-pVTZ orbital basis set, together with the def2/J auxiliary basis set (as implemented in the ORCA program) for the Hartree-Fock part and cc-pVTZ/C[14] auxiliary basis for the correlation part. The silver atom was described by the cc-pwCVTZ[15] orbital basis set in conjunction with the general SARC/J[16] auxiliary basis set for the RI-HF part and the cc-pwCVTZ/C[17] auxiliary basis set for the RI correlation integrals. All the quantum mechanical calculations were performed using the ORCA software.[18]

According to QTAIM topological features of the electron density, $\rho(r)$, can reveal important details about the structure of a molecule, using built concepts of atoms, bonds and some structural parameters.[8] For instance, the critical points of the electron density (CPs), where the first derivatives of $\rho(r)$ with respect to the geometry coordinates are zero, together with their curvatures (second derivatives in all directions) reveal some important interactions in the molecule of interest. The curvature of a CP is negative at a maximum and positive at a minimum and its value and algebraic sign taken from all three directions in space indicate the CP type. In the present work, only the (3,-1) CP type, which has three nonzero curvatures and for which the sum of algebraic values is -1, were

analyzed. This CP type indicates the presence of a chemical bond and has the property of electron density accumulation in the plane perpendicular to the axis linking two atomic nuclei.[8]

The (3,-1) CPs were determined for all complexes, not only in their equilibrium geometry, but in all points generated on the calculated potential energy surfaces using the MP2 relaxed electron densities. This indicates, within the QTAIM formalism, the presence of a chemical bond between these two atoms even for the large distances found at the minimum geometries, in which the two atoms are separated by distances around 2.65 Å. In the equilibrium geometries, calculations also show CPs between both oxygens of the nitrate and the silver atom, indicating that NO_3^- coordinates to the Ag center in a bidentate fashion, although the second coordination is not very stable.

Once the critical points are found, several properties calculated at the critical point provide important information on the nature of the interaction. The Laplacian of the electron density, $\nabla^2\rho(r)$, determines if $\rho(r)$ is locally accumulated, when $\nabla^2\rho(r) < 0$ and there is a local maximum of the electron density, or locally depleted, when $\nabla^2\rho(r) > 0$ and there is a local minimum. The Laplacian of $\rho(r)$ can be related to a local expression of the Virial theorem[8,19] as given in equation 1.

$$\frac{\hbar^2}{4m}\nabla^2\rho(r) = 2G(r) + V(r) \qquad (1)$$

In this expression, $G(r)$ is the electronic kinetic energy density and is always positive, while $V(r)$ is the potential energy density which is always negative. So, when the Laplacian is negative in a given CP or region, we have a local dominance of the potential energy density term, resulting in more localized electrons and an accumulation of charge, which characterizes a more covalent interaction.

On the other hand, when the Laplacian is positive, the kinetic term dominates the expression and there is a local depletion of the electron density. In a paired interaction, this means that the electrons concentrate charge near the bonded atoms rather than between the nuclei, resulting in the dominance of the kinetic energy. This happens in ionic, hydrogen-bond, and van der Waals interactions, and can be either attractive or repulsive. To better understand these terms, it is common

to introduce another quantity to determine the nature of the interaction between two atoms, the energy density *H(r)*, shown in equation 2.

$$H(r) = G(r) + V(r) \quad (2)$$

The local value of the energy density is determined by the electron energy density itself. When *H(r)* is negative, there is a predominance of the *V(r)* term contribution and it indicates covalent interactions. When *H(r)* is close to zero or positive, the kinetic energy term has a more prominent contribution and the bond tends to have more ionic character or to be hydrogen bond, van der Waals or other long-range interactions.

In the QTAIM analyses, bond paths are trajectories, connecting two atoms and a (3,-1) CP, in which the electronic density is a maximum with respect to any neighboring atoms.[20] The magnitude of electron density accumulation in a plane of a bond path compared to other planes perpendicular to it is given by the ellipticity, $\varepsilon(r)$, of a bond[19,20] The ellipticity is a good indicator of the stability of the bond. Usually, stable bonds have low values of ε, rather smaller than 1. As examples, $\varepsilon = 0.23$ between bonded carbons of benzene and $\varepsilon = 0.45$ in ethene, being very close to 0 in simple σ bonds as there is no preferential plane to accumulate electron density. Another useful function of the electronic density is the *eta index*, $\eta(r) = |\lambda_1|/\lambda_3$, which is the ratio between the lowest and largest eigenvalues from the Hessian matrix of $\rho(r)$. $\eta(r)$ is smaller than unity for closed-shell interactions and increases with increasing covalent character.[21,22]

References

(1) Parr, R. G.; Yang, W. Density-functional theory of atoms and molecules. Oxford University Press: New York, 1989; pp 1–333.

(2) Becke, A. D.; Density-Functional Thermochemistry. III. The Role of Exact Exchange Ab Initio Effective Core Potentials for Molecular Calculations. Potentials for K to Au Including the Outermost Core Orbitals Self-Consistent Molecular Orbital Methods. XX. A Basis Set for

Correlated Wave Functions Ab Initio Effective Core Potentials for Molecular Calculations. Potentials for the Transition Metal Atoms Sc to Density-Functional Thermochemistry. The Role of Exact Exchange. *J. Chem. Phys.* **1993**, *98*, 5648–5652.

(3) Weigend, F.; Ahlrichs, R. Balanced basis sets of split valence, triple zeta valence and quadruple zeta valence quality for H to Rn: Design and assessment of accuracy. *Phys. Chem. Chem. Phys.* **2005**, *7*, 3297–3305.

(4) Andrae, D.; Häußermann, U.; Dolg, M.; Stoll, H.; Preuß, H. Energy-adjusted ab initio pseudopotentials for the second and third row transition elements. *Theor. Chim. Acta*. **1990**, *77*, 123–141.

(5) Neese, F. An improvement of the resolution of the identity approximation for the formation of the Coulomb matrix. *J. Comput. Chem*. **2003**, *24*, 1740–1747.

(6) Neese, F.; Wennmohs, F.; Hansen, A.; Becker, U. Efficient, approximate and parallel Hartree–Fock and hybrid DFT calculations. A "chain-of-Spheres" algorithm for the Hartree–Fock exchange. *Chem. Phys*. **2009**, *356*, 98–109.

(7) Weigend, F. Accurate Coulomb-fitting basis sets for H to Rn. *Phys. Chem. Chem. Phys*. **2006**, *8*, 1057–1065.

(8) Bader, R. F. W. Atoms in Molecules. In Encyclopedia of Computational Chemistry; John Wiley & Sons, Ltd: Chichester, 2002; pp. 1–23.

(9) Lu, T.; Chen, F. Multiwfn: A multifunctional wavefunction analyzer. *J. Comput. Chem*. **2012**, *33*, 580–592.

(10) Grimme, S. Improved second-order Møller–Plesset perturbation theory by separate scaling of parallel- and antiparallel-spin pair correlation energies. *J. Chem. Phys*. **2003**, *118*, 9095–9102.

(11) Møller, C.; Plesset, M. S. Note on an approximation treatment for many-electron systems. *Phys. Rev.* **1934**, *46*, 618–622.

(12) Reiher, M. Douglas-Kroll-Hess Theory: a relativistic electrons-only theory for chemistry. *Theor. Chem. Acc.* **2006**, *116*, 241–252.

(13) Nakajima, T.; Hirao, K. The Douglas-Kroll-Hess approach. *Chem. Rev.* **2012**, *112*, 385–402.

(14) Weigend, F.; Köhn, A.; Hättig, C. Efficient use of the correlation consistent basis sets in resolution of the identity MP2 calculations. *J. Chem. Phys*. **2002**, *116*, 3175–3183.

(15) Peterson, K. A.; Puzzarini, C. Systematically convergent basis sets for transition metals. II. Pseudopotential-Based correlation consistent basis sets for the group 11 (Cu, Ag, Au) and 12 (Zn, Cd, Hg) elements. *Theor. Chem. Acc*. **2005**, *114*, 283–296.

(16) Orca 4.0 Basis Sets. Orca 4.0 Manual, 2017.

(17) Hattig, C. Auxiliary Basis Sets for RI-MP2 Calculations. TURBOMOLE basis set library 6.0, 2009.

(18) Neese, F. Software Update: The ORCA Program System, Version 4.0. *Wiley Interdiscip. Rev. Comput. Mol. Sci.* **2017**, e1327.

(19) Bader, R. F. W. A Quantum theory of molecular structure and its applications. *Chem. Rev.* **1991**, *91*, 893–928.

(20) Bader, R. F. W. A bond path: a universal indicator of bonded interactions. *J. Phys. Chem. A.* **1998**, *102*, 7314–7323.

(21) Amezaga, N. J. M.; Pamies, S. C.; Peruchena, N. M.; Sosa, G. L. Halogen bonding: a study based on the electronic charge density. *J. Phys. Chem. A.* **2010**, *114*, 552–562.

(22) Niepötter, B.; Herbst-Irmer, R.; Kratzert, D.; Samuel, P. P.; Mondal, K. C.; Roesky, H. W.; Jerabek, P.; Frenking, G.; Stalke, D. Experimental charge density study of a silylone. *Angew. Chem. Int. Ed. Engl.* **2014**, *53*, 2766–2770.